axioms

MDPI

Article

Analysis of Thermal Mixing and Entropy Generation during Natural Convection Flows in Arbitrary Eccentric Annulus

Satyvir Singh [1,2,*], Bidesh Sengupta [3] and Seetu Rana [4]

[1] Applied and Computational Mathematics, RWTH Aachen University, 52062 Aachen, Germany
[2] Department of Mathematics, Graphic Era Deemed to be University, Dehradun 248002, India
[3] Department of Physics and Astronomy, University of Bologna, 40126 Bologna, Italy; bidesh.sengupta@unibo.it
[4] Department of Mathematics, Government College Hisar, Hisar 125001, India; seetuduhan23@gmail.com
* Correspondence: singh@acom.rwth-aachen.de; Tel.: +49-162-4707-356

Abstract: The present study presents a computational investigation into the thermal mixing along with entropy generation throughout the natural convection flow within an arbitrarily eccentric annulus. Salt water is filled inside the eccentric annulus, in which the outer and inner cylinders have T_c and T_h constant temperatures. The Boussinesq approximation is used to develop the governing equations for the natural convection flow, which are then solved on a structured quadrilateral mesh using the OpenFOAM software package (FOAM-Extend 4.0). The computational simulations are performed for Rayleigh numbers ($Ra = 10^3$–10^5), eccentricity ($\epsilon = 0,\ 0.4,\ 0.8$), angular positions ($\varphi = 0°,\ 45°,\ 90°$), and Prandtl number ($Pr = 10$, salt water). The computational results are visualized in terms of streamlines, isotherms, and entropy generation caused by fluid friction and heat transfer. Additionally, a thorough examination of the variations in the average and local Nusselt numbers, circulation intensity with eccentricities, and angular positions is provided. The optimal state of heat transfer is shown to be influenced by the eccentricity, angular positions, uniform temperature sources, and Boussinesq state. Moreover, the rate of thermal mixing and the production of total entropy increase as Ra increases. It is found that, compared to a concentric annulus, an eccentric annulus has a higher rate of thermal mixing and entropy generation. The findings show which configurations and types of eccentric annulus are ideal and could be used in any thermal processing activity where a salt fluid ($Pr = 10$) is involved.

Keywords: natural convection; OpenFOAM simulations; eccentric annulus; isotherms; streamlines; entropy generation

MSC: 80A20; 74S10; 76A02; 76E06; 76Rxx

Citation: Singh, S.; Sengupta, B.; Rana, S. Analysis of Thermal Mixing and Entropy Generation during Natural Convection Flows in Arbitrary Eccentric Annulus. *Axioms* **2024**, *13*, 233. https://doi.org/10.3390/axioms13040233

Academic Editor: Gabriella Bretti

Received: 7 February 2024
Revised: 15 March 2024
Accepted: 23 March 2024
Published: 1 April 2024

1. Introduction

In fluid mechanics, a natural convection flow is a type of heat transfer whereby fluid movement arises from the density differences within a fluid due to temperature variations. A fluid rises when heated because it expands and loses density. Conversely, when it is cooled, it contracts and becomes denser, leading it to sink. This spontaneous fluid movement caused by buoyancy forces brought about by density gradients produces a natural flow pattern known as natural convection. Notably, there are no external mechanical devices driving the fluid motion in such flows. Owing to the considerable number of applications in diverse industries and scientific domains, studies on natural convection heat transport in circular and eccentric enclosures, like pipes, tubes, or cylinders, have garnered significant attention from both academia and industry. Some notable applications include the design and analysis of wellbores and pipelines, the oil and gas industry, cooling systems, underground electric cables, solar water heaters, nuclear reactor cooling, food processing, geothermal energy systems, chemical reactors, and many more [1–7]. For instance, in drilling operations, wellbores are often drilled through geological formations

to extract oil or gas. During this process, the wellbore may not always be perfectly centered within the surrounding casing or formation, leading to an eccentric annulus. The above-mentioned applications highlight the importance of understanding and utilizing natural convection within annular enclosures in various engineering and scientific contexts.

In 1931, Beckmann [8] introduced the first experimental study of horizontal annular enclosures. For the first time, in 1961, Crawford and Lemlich [9] introduced two-dimensional computational simulations to solve steady-state laminar natural convection flows inside horizontal concentric cylinders utilizing finite difference schemes. In their study, numerical simulations were visualized through streamlines and isotherm contours for $Pr = 0.714$. In 1964, Abbott [10] presented the numerical results for a narrow, horizontally aligned concentric cylindrical annulus by solving the conservation laws for laminar natural convection flows at steady state with flow parameters $Gr = 10^{10}$ and $Ra = 10^3$. Later, Mack and Bishop [11] investigated two-dimensional natural convection at steady state within horizontal concentric cylinders for low Rayleigh numbers ($Ra = 300,\ 3000$) with varing Prandtl numbers ($0.02 \leq Pr \leq 0.70$). They illustrated the numerical results through the isotherms and streamlines and found that Pr had a higher-order effect on the total heat transport; it only arose for the fourth and higher powers of Ra. Moukalled and Acharya [12] demonstrated numerical solutions for natural convection thermal mixing in a heated horizontal cylinder positioned concentrically within a square enclosure with $Pr = 0.71$, $10^3 \leq Ra \leq 10^7$ and different aspect ratios.

Extensive research has been carried out the natural convection thermal mixing in a horizontally aligned cylindrical annulus, spurred by the previously described investigations. Powe et al. [13] studied the natural convection within horizontal cylindrical annuli for $Pr = 0.71$. Kuehn and Goldstein [14] carried out both numerical and experimental studies on the natural convection thermal mixing inside a horizontal annulus to expand the understanding of the velocity and temperature distributions as well as the local heat transfer coefficients. For a wide range of Ra, from conduction to the steady flow phase dominated by convection, Kumar [15] numerically investigated the natural convection thermal mixing of fluids in horizontally aligned annulus enclosures. The findings predicted that the heat transfer rate would increase with an enlargement in Ra based on the same temperature differential for the inner cylinder with a constant heat flux. Labonia and Guj [16] conducted an experimental study of the transition from a steady laminar to a chaotic flow in a horizontal annulus between concentric cylinders for $0.90 \times 10^5 \leq Ra \leq 3.37 \times 10^5$. Later, Dyko et al. [17] reported an investigation into the natural convection flows inside a horizontal cylindrical annulus at Ra approaching and above the critical values using both numerical and experimental methods. Shahrani and Zeitoun [18] performed a numerical analysis of the natural convection thermal mixing between two horizontal concentric cylinders with two fins attached to the inner cylinder using the finite element method. They demonstrated that the thermal resistance declined as the fin length increased. Subsequently, Teertstra et al. [19] created an analytical model to analyze the natural convection thermal mixing in concentric spherical enclosures. The convective component of this model was determined by combining the two limiting situations of laminar boundary layer convection and transition flow convection, which involved the linear superposition of conduction and convection solutions. Sankar et al. [20] quantitatively examined the natural convection of an electrically conducting fluid in the presence of an axial or radial magnetic field in a vertical cylindrical annulus with a low Prandtl number ($Pr = 0.054$). The findings demonstrate that in shallow cavities, an axial magnetic field effectively controls the flow and heat transmission, whereas, in tall cavities, a radial magnetic field accomplishes this. Recently, Alsabery et al. [21] illustrated finite-element-based numerical simulations of the natural convection thermal mixing of a blood-filled horizontally aligned concentric annulus. According to this study, a low power-law index enhances the heat transfer rate and fluid flow. Rana et al. [22] reported OpenFOAM-based steady-state numerical simulations to investigate the natural convection thermal mixing inside a horizontally aligned concentric annulus at constant temperatures.

In contrast to the concentric cylindrical annulus, there is comparatively less research on the natural convection between two eccentric cylinders. Generally, these studies have been focused on the annuli between two eccentric cylinders that are either vertically or horizontally oriented. Trombetta [23] investigated the energy equation solutions that met specific fundamental boundary requirements for laminar forced convection thermal mixing flows in eccentric annuli. Later, Kuehn and Goldstein [24] conducted an experimental study to determine the impacts of the eccentricity, rotation angle, and Rayleigh number ($2.2 \times 10^2 \leq Ra \leq 7.7 \times 10^7$) on the natural convection thermal mixing in concentric and eccentric horizontal cylindrical annuli. Chakrabarti et al. [25] determined the geometrical arrangements of the air-filled, horizontal eccentric annuli that offered the highest level of thermal insulation in accordance with different temperature constraints. In an annulus between two eccentric horizontal isothermal tubes, Badr [26] investigated numerically the laminar free convective thermal mixing for various diameter ratios and $0 \leq Ra \leq 10^4$. This work demonstrates that, for smaller-diameter annuli, eccentricity still has a significant impact on the total thermal mixing coefficient throughout a larger range of Ra. Prusa and Yao [27] studied numerically the laminar natural convection thermal mixing in both vertically and horizontally aligned eccentric cylinders. The findings show that while the buoyancy increases with the Grashof number, eccentricity still has a major impact on the thermal mixing and flow fields in eccentric cylinders. Moreover, buoyancy boosts the average heat transfer. For a steady-state, laminar natural convection flow, Guj and co-authors [28,29] carried out both experimental and numerical studies on the thermal mixing and heat transfer in a two-dimensional horizontally eccentric annulus. The findings show that the inner cylinder's horizontal eccentricity significantly changes the thermal field and plume shape, while also providing, contrary to established numerical conclusions, a non-zero azimuthal flow rate in the channel between the two cylinders. Following this, Shu et al. [30] conducted a systematic examination of the impact of the eccentricity and angular position on the flow and thermal fields by numerically studying the natural convective thermal mixing in a horizontal eccentric annulus. In an annulus formed between two horizontal eccentric circular cylinders, Mahfouz [31] predicted numerically the natural convection thermal mixing. In their study of free convection in horizontal concentric annuli with varied inner shapes (cylindrical, elliptical, square, or triangular), Yuan et al. [32] demonstrated the flow and thermal fields using streamlines and isotherms. In a recent study, Talukdar and Tsubokura [33] presented numerical results regarding how the aspect ratio of a cooled square outer enclosure and the cylinder's position at high Ra affected the natural convection thermal mixing characteristics of a stationary 2D horizontal cylinder. Shahsavar et al. [34] examined the hydrothermal features based on the first and second laws of thermodynamics in a naturally cooled eccentric horizontal annulus filled with a non-Newtonian nanofluid. Al-Sumaily et al. [35] presented a numerical analysis of the effects of the sphere diameter and porosity on the natural convection thermal mixing inside an eccentric annulus packed with stationary spheres.

Most of the eccentric annulus applications described above are closely related to energy consumption. The goal when constructing any thermal system is to use valuable resources as efficiently as possible. Therefore, it is necessary to analyze natural convection in an energy-efficient manner in order to potentially optimize the energy inside a system. Despite the availability of numerous advanced optimization techniques, entropy generation minimization (EGM) [36] is a rather practical method for the analysis and maximization of energy systems in engineering applications. The effectiveness of the EGM method stems from its ability to provide a clear understanding of the irreversibilities that control a system's efficiency by adding concepts from fluid mechanics and thermal mixing to the second law of thermodynamics. As a result, EGM is of significant interest in thermal mixing and receives a lot of attention from researchers. The extensive range of applications makes the research of entropy generation resulting from natural convection thermal mixing in concentric and eccentric annulus particularly significant. Mahmud and Fraser [37] examined the features of the fluid flow and heat mixing inside a cylindrical annulus using

entropy generation based on the first and second laws (of thermodynamics). According to their research, if the inner cylinder rotated more than the outer, the entropy generation rate would exhibit asymptotic behavior close to the outer cylinder. In the entry region of a concentric cylindrical annulus, Haddad et al. [38] examined the entropy generated by laminar forced convection thermal mixing and discovered that thermal entropy generation was comparatively more prominent than viscous entropy generation. Yari [39] focused on improving the thermal mixing efficiency along with the fluid flows within a microannulus, and they discovered that as the Knudsen number increased, the entropy generation was reduced. For natural convection inside a vertically concentric annulus, Chen et al. [40] methodically examined the impacts of Ra, the annulus's curvature, and Pr on the flow pattern, temperature distribution, and entropy generation. Nevertheless, to the best of the authors' knowledge, no prior attempt has been made to investigate the thermal mixing and entropy generation that occurs during the natural convection flows within an arbitrarily eccentric annulus. Therefore, efforts must be made to improve the knowledge of the irreversibilities of the fluid flow and thermal mixing during natural convection flows inside arbitrarily eccentric annuli.

The primary aim of the present research is to investigate the entropy generation caused by heat transfer and fluid friction, and the fluid flow and thermal mixing, in the natural convection process inside an arbitrary eccentric annulus filled with an incompressible fluid subject to the thermal uniform boundary condition. The aim is also to investigate and evaluate the roles that the inner cylinder eccentricity and angular position play in enhancing the thermal mixing and reducing entropy formation. For this purpose, OpenFOAM, an open-source computational fluid dynamics software tool, is utilized to solve the highly nonlinear Navier–Stokes equations related to the flow fields, thermal mixing, and mechanism of entropy generation. Numerical simulations are conducted for various parameters: the Prandtl number ($Pr = 10$, salt water), Rayleigh numbers ($10^3 \leq Ra \leq 10^5$), inner cylinder eccentricities ($\epsilon = 0,\ 0.4,\ 0.8$), and angular positions ($\varphi = 0^\circ,\ 45^\circ,\ 90^\circ$). Salt water is typically used in heat and mass transfer processes due to its unique properties, such as its higher thermal conductivity and ability to absorb or release large amounts of heat. The contours of the isotherms, streamlines, entropy generation from heat transfer, and fluid friction are used to describe the numerical simulation findings. Additionally, the implications of the eccentricity, angular location, and Rayleigh number on the entropy generation as a result of fluid and thermal irreversibilities are discussed. As part of the natural convection process, an analysis was also performed to evaluate the average and local Nusselt values.

2. Mathematical Formulation

2.1. Problem Setup

In this study, we investigate the laminar natural convection flow in two dimensions at steady state in an incompressible Newtonian fluid embedded in an arbitrary eccentric cylindrical annulus. A schematic diagram of the natural convection thermal mixing problem in an annulus formed within two long horizontal eccentric cylinders and the mesh point distribution is illustrated in Figure 1. In this diagram, R_o and R_i are the radii of the outer and inner cylinders, respectively. The geometric relationship between the outer and inner cylinders may be delineated by the eccentricity ($\epsilon \leq L$, where $L = R_o - R_i$) and angular positions ($0^\circ \leq \varphi \leq 90^\circ$). In this study, the outer and inner cylinders have uniform temperatures of $T_o = 288$ K and $T_i = 298$ K, respectively, with the condition $T_i > T_o$. In this arrangement, the outer cylinder can be regarded as the cold wall and the inner cylinder as the hot wall. We assume that the salt fluid fills the eccentric annulus in this case. For the numerical simulations, we set $L/R_i = 1.6$. Additionally, the gravitational force g is configured in the negative y-direction. The presence of a temperature gradient leads to the thermal expansion of the fluid in the domain. This leads to a buoyancy-induced flow, which in turn causes natural convection.

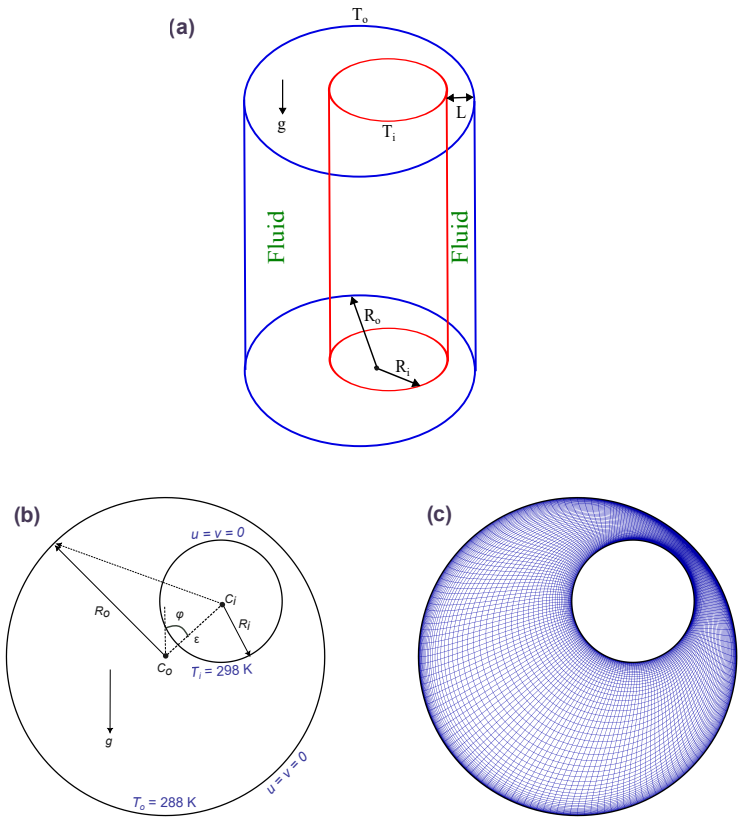

Figure 1. Schematic representation of the physical system in (**a**) three dimensions and (**b**) two dimensions. (**c**) Structured quadrilateral mesh.

2.2. Governing Equations

In this study, two-dimensional numerical simulations are conducted by solving the mass, momentum under Boussinesq approximation, and energy equations for the steady-state natural convection flow within an arbitrary eccentric annulus. These equations can be written as follows:

$$\frac{\partial u}{\partial x} + \frac{\partial v}{\partial y} = 0, \tag{1}$$

$$u\frac{\partial u}{\partial x} + v\frac{\partial u}{\partial y} = -\frac{1}{\rho}\frac{\partial p}{\partial x} + \mu\left(\frac{\partial^2 u}{\partial x^2} + \frac{\partial^2 u}{\partial y^2}\right), \tag{2}$$

$$u\frac{\partial v}{\partial x} + v\frac{\partial v}{\partial y} = -\frac{1}{\rho}\frac{\partial p}{\partial y} + \nu\left(\frac{\partial^2 v}{\partial x^2} + \frac{\partial^2 v}{\partial y^2}\right) + g\beta(T - T_c), \tag{3}$$

$$u\frac{\partial T}{\partial x} + v\frac{\partial T}{\partial y} = \alpha\left(\frac{\partial^2 T}{\partial x^2} + \frac{\partial^2 T}{\partial y^2}\right). \tag{4}$$

The corresponding boundary conditions are given below:

$$\begin{aligned} u = 0,\ v = 0,\ T = T_c \text{ at } r = R_o, \\ u = 0,\ v = 0,\ T = T_h \text{ at } r = R_i, \end{aligned} \tag{5}$$

where (x, y) are the rectangular Cartesian coordinates; (u, v) are the corresponding velocity components; T denotes the temperature; ν and α are the kinematic viscosity and thermal conductivity, respectively; p is the pressure; ρ is the density; and T_h and T_c are the temperature in the hot inner cylinder and cold outer cylinder, respectively.

Using the following change of variables,

$$X = \frac{x}{L},\ y = \frac{y}{L},\ U = \frac{uL}{\alpha},\ V = \frac{vL}{\alpha},\ \theta = \frac{T - T_c}{T_h - T_c},$$
$$P = \frac{pL^2}{\rho\alpha^2},\ Pr = \frac{\nu}{\alpha},\ Ra = \frac{g\beta(T_h - T_c)L^3 Pr}{\nu^2} \tag{6}$$

the governing Equations (1)–(5) are reduced to a non-dimensional form,

$$\frac{\partial U}{\partial X} + \frac{\partial V}{\partial Y} = 0, \tag{7}$$

$$U\frac{\partial U}{\partial X} + V\frac{\partial U}{\partial Y} = -\frac{\partial P}{\partial X} + Pr\left(\frac{\partial^2 U}{\partial X^2} + \frac{\partial^2 U}{\partial Y^2}\right), \tag{8}$$

$$U\frac{\partial V}{\partial X} + V\frac{\partial V}{\partial Y} = -\frac{\partial P}{\partial Y} + Pr\left(\frac{\partial^2 V}{\partial X^2} + \frac{\partial^2 V}{\partial Y^2}\right) + Ra\,Pr\,\theta, \tag{9}$$

$$U\frac{\partial \theta}{\partial X} + V\frac{\partial \theta}{\partial Y} = \frac{\partial^2 \theta}{\partial X^2} + \frac{\partial^2 \theta}{\partial Y^2}. \tag{10}$$

with the boundary conditions

$$U = 0,\ V = 0,\ \theta = 0 \text{ at } r = R_o,$$
$$U = 0,\ V = 0,\ \theta = 1 \text{ at } r = R_i. \tag{11}$$

In the above-mentioned equations, (U, V) are the dimensionless velocity components in the dimensionless rectangular Cartesian coordinates (X, Y); θ is the dimensionless temperature; P is the dimensionless pressure; Ra and Pr represent the Rayleigh and Prandtl numbers, respectively; β denotes the thermal expansion coefficient; and L represents the characteristic length chosen as the gap within an eccentric cylindrical annulus, i.e., $L = R_o - R_i$.

2.3. Heat Transfer Parameters

2.3.1. Streamfunction

The streamfunction (ψ), which is derived from the velocity components (U, V), is used to depict the fluid motion. For two-dimensional flows, the relationships between the streamfunction and velocity components are

$$U = \frac{\partial \psi}{\partial Y} \quad \text{and} \quad V = -\frac{\partial \psi}{\partial X}, \tag{12}$$

which produce a solitary equation:

$$\frac{\partial^2 \psi}{\partial X^2} + \frac{\partial^2 \psi}{\partial Y^2} = \frac{\partial U}{\partial Y} - \frac{\partial V}{\partial X}. \tag{13}$$

According to the definition of the streamfunction given above, the positive sign of ψ indicates circulation that is moving counter-clockwise, and the negative sign of ψ indicates circulation that is moving clockwise.

2.3.2. Nusselt Numbers

After the distributions of the streamfunction and isotherms are generated, the characteristics of flow and heat transport may be readily determined. The streamfunction distribution facilitates the plotting of the flowfield in terms of streamlines and the determination of the flow velocity, while the isotherm distribution helps to locate the heat transfer

findings in terms of local and mean Nusselt numbers. At the inner and outer cylinders, the local Nusselt number is defined as

$$\begin{aligned} Nu_{lo}^{in} &= -\left(\frac{\partial T}{\partial S_n}\right)_i \frac{D_i}{(T_i - T_o)}, \\ Nu_{lo}^{ou} &= -\left(\frac{\partial T}{\partial S_n}\right)_o \frac{D_o}{(T_i - T_o)}, \end{aligned} \tag{14}$$

where D_o and D_i denote the diameters of the outer and inner cylinders, respectively. S_n is the heat flux normal to the wall in the local direction. For the inner and outer cylinders, the average (mean) Nusselt numbers are given by

$$\begin{aligned} Nu_{av}^{in} &= \frac{1}{2\pi}\int_0^{2\pi} Nu_{lo}^{in} dP_{in}, \\ Nu_{av}^{ou} &= \frac{1}{2\pi}\int_0^{2\pi} Nu_{lo}^{ou} dP_{ou}, \end{aligned} \tag{15}$$

where P_{in} and P_{ou} are the perimeters of the inner and outer cylinders, respectively.

2.3.3. Entropy Generation

The associated irreversibilities in natural convection systems are caused by fluid friction and heat transfer [36]. The dimensionless local entropy generation for two-dimensional heat and fluid movement in Cartesian coordinates (X, Y) in explicit form is as follows from the local thermodynamic equilibrium based on the hypothesis of linear transport:

$$S_{\theta,l} = \left[\left(\frac{\partial \theta}{\partial X}\right)^2 + \left(\frac{\partial \theta}{\partial Y}\right)^2\right], \tag{16}$$

and

$$S_{\psi,l} = \phi\left\{2\left[\left(\frac{\partial U}{\partial X}\right)^2 + \left(\frac{\partial U}{\partial Y}\right)^2\right] + \left(\frac{\partial U}{\partial X} + \frac{\partial V}{\partial X}\right)^2\right\}, \tag{17}$$

where the local entropy production resulting from heat transfer and fluid friction, respectively, is denoted by $S_{\theta,l}$ and $S_{\psi,l}$. The term ϕ in the equation above refers to the irreversibility distribution ratio, which is defined as

$$\phi = \frac{\mu T_0}{\kappa}\left(\frac{U_0}{\Delta T}\right)^2, \tag{18}$$

For the sake of this study, ϕ is 10^{-3}. A comparable outcome would also be obtained from an order of magnitude study. At 298 K, for instance, the order of magnitude of water is $\mu \sim O(10^{-3})$ and $\kappa \sim O(10^{-1})$. In a representative situation, $T_0/\Delta T^2 \sim O(10)$, and $O(10^{-3})$ is found for ϕ. The bulk temperature, T_0, is calculated as $(T_h + T_c)/2$ in this study.

3. Numerical Implementation, Mesh Independence, and Validation Studies

3.1. Numerical Implementation

In this study, the modified 'buoyantBoussinesqSimpleFoam' solver, which is a component of the open-source C++ libraries of OpenFOAM (Open Field Operation and Manipulation) [41], is utilized to carry out the numerical simulations. OpenFOAM is a free and open-source computational fluid dynamics (CFD) software program that provides a comprehensive range of CFD solvers and utilities for the simulation of fluid flows, heat transfer, chemical reactions, and other related phenomena. The software is extensively used in academia, research, and industry to simulate and analyze complex fluid flow problems. This solver uses a finite volume approach to solve a general system of partial differential equations. It is an excellent and well-known open-source CFD tool that has several benefits, including no license fees, easy code customization, a meshing tool, and mesh processing

routines that are fully equipped for MPI parallelization, as well as the ability to link with external codes. Due to these features, we choose OpenFOAM over other CFD programs for the present study. Numerical solutions are interpolated onto the uniform meshes for flow field visualization, and graphic methods like Tecplot 360 are utilized for this purpose.

3.2. Mesh Independence Study

Based on a thorough examination of four distinct uniform quadrilateral meshes, 'Mesh 1–Mesh 4', the mesh independence of the numerical findings is demonstrated for the case of $Pr = 10$, $Ra = 10^4$, $\epsilon = 0$, and $\varphi = 0^\circ$. Table 1 provides pertinent information about the total elements, total nodes, and maximum skewness for the considered meshes. It can be obtained from the table that when the mesh size is above 'Mesh 3', the computed average Nussult numbers for inner and outer cylinders $(Nu_{av}^{in}, Nu_{av}^{ou})$ and circulation intensity $(|\psi|_{max})$ remain unchanged. Thus, all numerical simulations are carried out using "Mesh 3", which offers an acceptable compromise between high accuracy and computational efficiency, in light of the previously indicated discussion.

Table 1. Mesh independence study for $Pr = 10$, $Ra = 10^4$, $\epsilon = 0$, and $\varphi = 0^\circ$.

Mesh Type	Total Elements	Total Nodes	Max Skewness	Nu_{av}^{in}	Nu_{av}^{ou}	$\|\psi\|_{max}$
Mesh 1	2352	2400	0.16447	3.3555	1.30274	13.21
Mesh 2	4802	4900	0.08069	3.3635	1.30115	12.89
Mesh 3	9702	9900	0.03990	3.3659	1.30972	12.26
Mesh 4	12,152	24,552	0.03181	3.3659	1.30972	12.26

3.3. Validation Study

To verify the reliability and accuracy of the employed OpenFOAM solver, two benchmark test cases are considered. As a first test case, the OpenFOAM results are compared with the experimental work of Guj and Stella [29] and the numerical results of Shu et al. [30], in which the eccentric annulus was filled with air ($Pr = 0.71$). The aforementioned experimental and numerical works were performed for $\epsilon = 0.5$, $Ra = 5.3 \times 10^3$, $L/D_i = 0.8$. Figure 2 illustrates the contour comparisons of the streamlines and isotherms between the experimental study of Guj and Stella [29], the numerical works of Shu et al. [30], and OpenFOAM. The present results reveal similar patterns for the streamline and isotherm generation observed in the previous experiments and the numerical results. Thus, the OpenFOAM results demonstrate strong qualitative agreement with the numerical and experimental findings.

In the second benchmark test scenario, a square enclosure is simulated for the parameters $Pr = 0.71$ and $Ra = 10^3$. In order to replicate the situation described by Singh et al. [42], this validation research was conducted for a differentially heated square cavity with a hot left wall and cool right wall in the presence of adiabatic top and bottom walls. In the study of Singh et al. [42], by maintaining the adjacent grid nodes at their respective wall temperatures and defining the average temperature of the two walls at the hot–cold junction points, the problem was overcome. In their investigation, a Gaussian quadrature-based finite element method was employed. The obtained contours of local entropy generation due to heat transfer S_θ and fluid friction S_ψ are compared here with the numerical results of Singh et al. [42], as illustrated in Figure 3. This figure shows that the entropy generation findings agree satisfactorily with the earlier work [42].

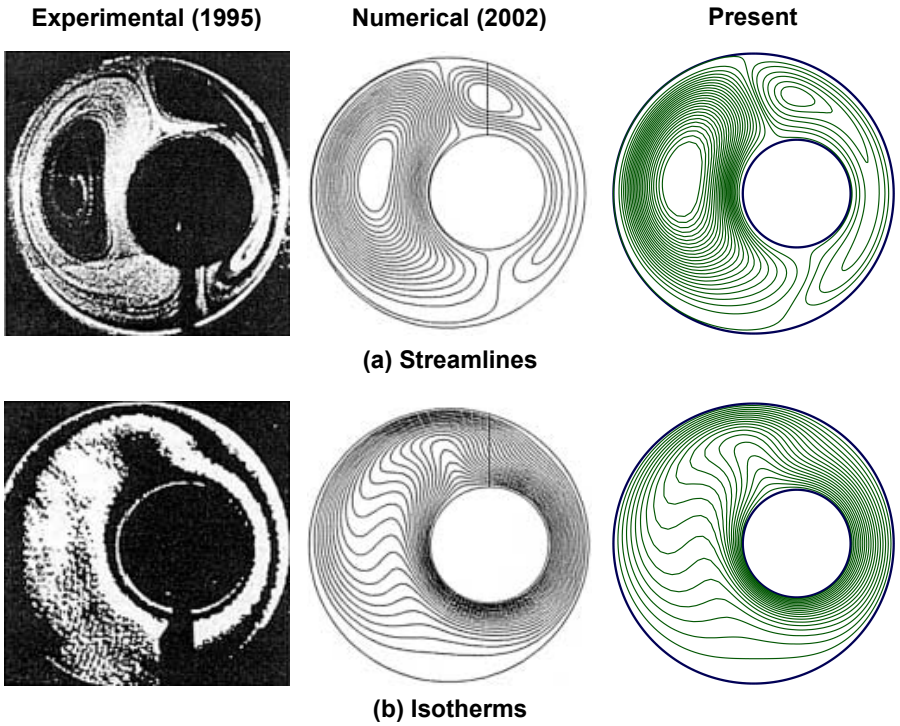

Figure 2. Validation study: comparison of (**a**) streamlines and (**b**) isotherm contours between the experimental work of Guj and Stella [29], the numerical works of Shu et al. [30] and the present OpenFOAM results for an eccentric annulus at $Pr = 0.71$, $\epsilon = 0.5$, and $Ra = 5.3 \times 10^3$.

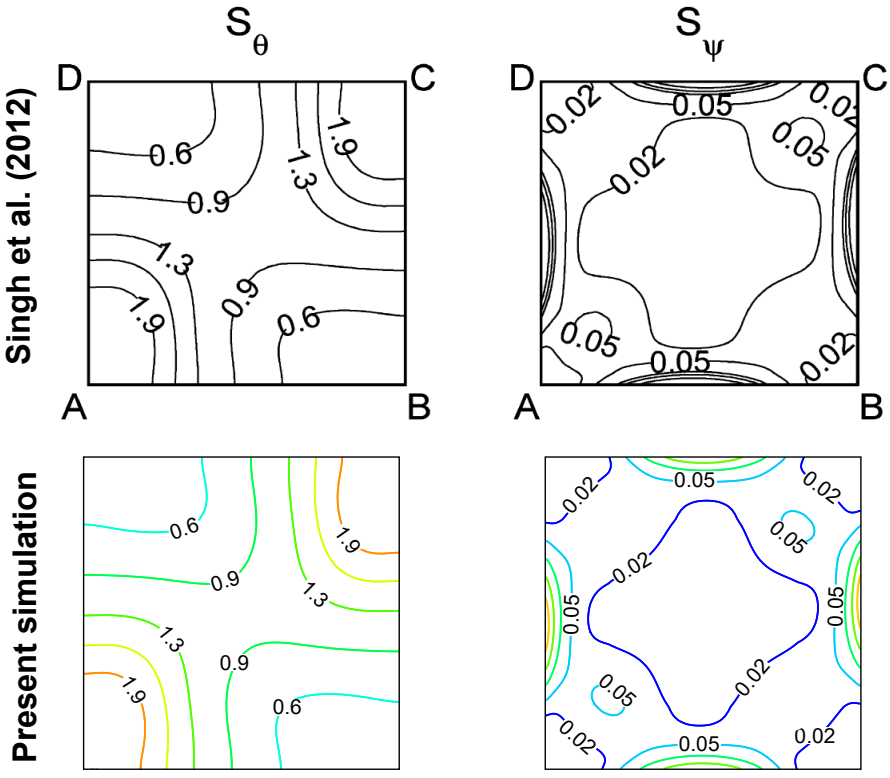

Figure 3. Validation study: comparison of local entropy generation due to heat transfer S_θ and fluid friction S_ψ between FEM simulation [42] and present OpenFOAM results for a square enclosure with the parameters $Pr = 0.71$, and $Ra = 10^3$.

4. Numerical Results and Discussion

This section provides a detailed analysis of the heat mixing and entropy generation during natural convection flows within an arbitrarily eccentric annulus. The considered eccentric annulus is filled with salt water ($Pr = 10$) For the numerical simulations, the following parameters are taken into account: eccentricity ($\epsilon = 0,\ 0.4,\ 0.8$), Rayleigh number ($10^3 \leq Ra \leq 10^5$), and angular position ($\varphi = 0^\circ,\ 45^\circ,\ 90^\circ$).

This section is divided into four parts: the impacts of the Ra numbers on thermal mixing and entropy generation in a concentric annulus are discussed in the first part. Subsequently, the effects of the φ and Ra numbers on entropy generation and heat transfer in an eccentric annulus at $\epsilon = 0.4$ are explored in the second part. Then, the impacts of the φ and Ra numbers on the thermal mixing and entropy generation in an eccentric annulus at $\epsilon = 0.8$ are investigated in the third part. Finally, the associated heat transfer parameters, including the local and average Nusselt numbers, and the circulation intensity are analyzed in the fourth part.

4.1. Case 1: Concentric Annulus with $\epsilon = 0$ and $\varphi = 0^\circ$

Figure 4 illustrates the contours of the isotherms (θ), the local entropy generation caused by thermal mixing ($S_{\theta,l}$), the streamlines (ψ), and the local entropy generation caused by fluid friction ($S_{\psi,l}$) of the concentric annulus for $\varphi = 0^\circ$, $\epsilon = 0$, $Pr = 10$ and $Ra = 10^3$–10^5. It is seen that the isotherms (θ) deviate from their circular curved shape, which indicates increasing heat convection and decreasing heat conduction, when Ra is increased for the concentric annulus scenario. In particular, at a smaller Ra ($Ra = 10^3$), conduction dominates the heat transfer in the annulus and the natural convection is very weak, which causes the isotherms to move up and alters their shapes. The hot fluid rises and generates plumes in the annulus when the Ra is raised to $Ra = 10^4$. Between the hot inner cylinder and the cold outer cylinder, the plume starts, and between these is a layer of cold fluid. Interestingly, both the width of the plume and the thickness of the cold layer decrease with the increase in Ra from 10^4 to 10^5. Consequently, the formed plume of cold fluid, which begins from the top of the cold outer cylinder and moves to the hot inner cylinder, is formed. This phenomenon is similar to Rayleigh–Benard convection. In light of this, the maximum local entropy generation ($S_{\theta,l,max}$) resulting from heat transfer is located close to the top and bottom portions of the outer and inner cylinders, with $S_{\theta,l,max} = 5.57$ for $Ra = 10^3$, $S_{\theta,l,max} = 22.83$ for $Ra = 10^4$, and $S_{\theta,l,max} = 60.38$ for $Ra = 10^5$.

Conversely, the magnitude of the streamfunction (ψ) allows one to observe the fluid flow inside the concentric annulus. It is observed that the natural convection flow is quite weak at a low Ra ($Ra = 10^3$) and that conduction is the main source of heat transfer. Thus, two symmetric vertices caused by natural convection can be observed. As expected, due to the cold outer walls, the fluids rise up from the middle portion of the inner wall and flow down along the outer walls, forming two symmetric rolls with clockwise and anti-clockwise rotations inside the concentric annulus. Moreover, the magnitude of the streamfunction is very low, i.e., $|\psi|_{max} = 2.2$. As Ra increases, the location of the configuration cell moves up. In addition, the magnitudes of the streamfunctions increase and are found to be $|\psi|_{max} = 12$ and 31 for $Ra = 10^4$ and $Ra = 10^5$, respectively. Because of the huge velocity gradient in the vicinity of the left and right sides of the inner and outer cylinders, wherein the circulation cells come into contact with the annulus, the entropy production resulting from the fluid friction is likewise very poor for $Ra = 10^3$. It is determined that, for $Ra = 10^3, 10^4$, and 10^4, respectively, the highest values of $S_{\psi,l}$ are 1.035, 52.88, and 1410.59 (see Figure 4). The distribution of $S_{\psi,l}$ in these places is indicated by the compact contours of S_ψ nearby the center part of the left and right sides of the inner and outer cylinders. Because there is a smaller velocity gradient here, some trivial S_ψ values are observed in the center of the concentric annulus for all Ra values.

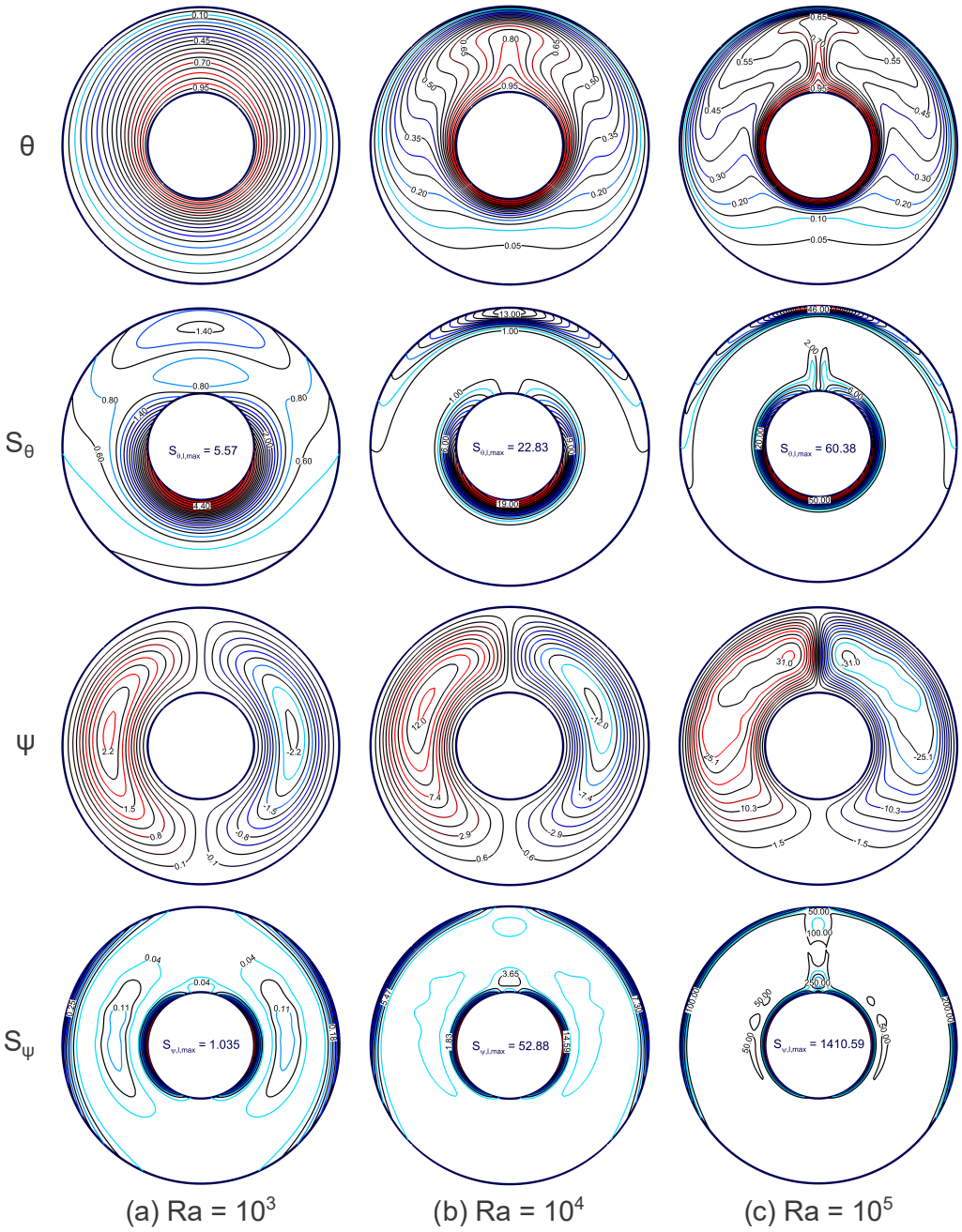

Figure 4. Contours of isotherms (θ), local entropy generation caused by heat transfer ($S_{\theta,l}$), stream-function (ψ), and local entropy generation caused by fluid friction ($S_{\psi,l}$) of the concentric annulus ($\varphi = 0$ and $\epsilon = 0$) for $Ra = 10^3$–10^5.

4.2. Case 2: Eccentric Annulus with $\epsilon = 0.4$ and $\varphi = 0°$, 45°, 90°

Figures 5 and 6 illustrate the contours of the isotherms (θ), the local entropy generation caused by thermal mixing ($S_{\theta,l}$), the streamlines (ψ), and the local entropy generation caused by fluid friction ($S_{\psi,l}$) of the eccentric annulus for $Pr = 10$, $\epsilon = 0.4$, $Ra = 10^3$–10^5 with different angular positions $\varphi = 0°, 45°, 90°$. For the case of a vertically eccentric annulus ($\varphi = 0°$), with an isothermally hot inner cylinder and cold outer cylinder, the fluid rises against gravity from the center of the inner cylinder due to buoyancy and rolls down the cold outer cylinder to generate two symmetric rolls inside the eccentric annulus cavity that rotate clockwise and counterclockwise. Regarding the eccentric annulus with certain angular positions ($\varphi \neq 0°$), the effect of both the tangential and normal components of the buoyancy force relative to the hot inner cylinder plays a critical role in both the flow and

thermal characteristics. As the angular position increases, the buoyancy force along the hot inner cylinder gradually increases, leading to stronger anticlockwise fluid circulation. This is also due to an increase in the tangential component of the buoyancy force, which is zero in the case of the vertically eccentric annulus ($\varphi = 0°$). Notably, the inner cylinder is always surrounded by a thermal boundary layer, while the presence of a boundary layer on the outer cylinder depends on the inner cylinder's position. When the inner cylinder is moved near the top with eccentricity, there is no boundary layer on the bottom portion of the outer cylinder. The results indicate that the fluid circulation, isotherms, and entropy generation are strongly dependent on the angular position (φ) as well as the eccentricity (ϵ) of the eccentric annulus.

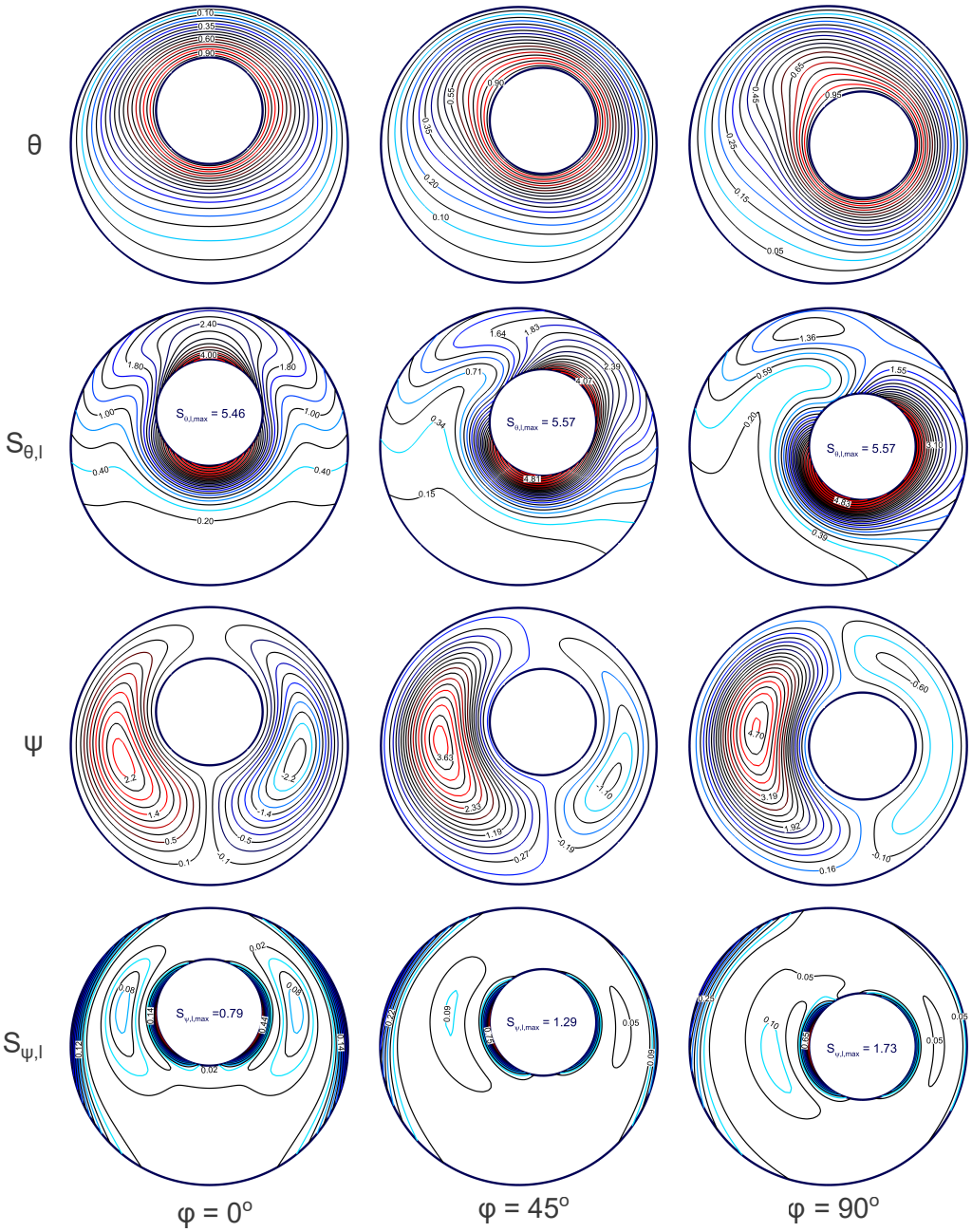

Figure 5. Contours of isotherms (θ), local entropy generation caused by thermal mixing ($S_{\theta,l}$), streamfunction (ψ), and local entropy generation caused by fluid friction ($S_{\psi,l}$) of an eccentric annulus for $\epsilon = 0.4$, $Ra = 10^3$ with different angular positions $\varphi = 0°, 45°, 90°$.

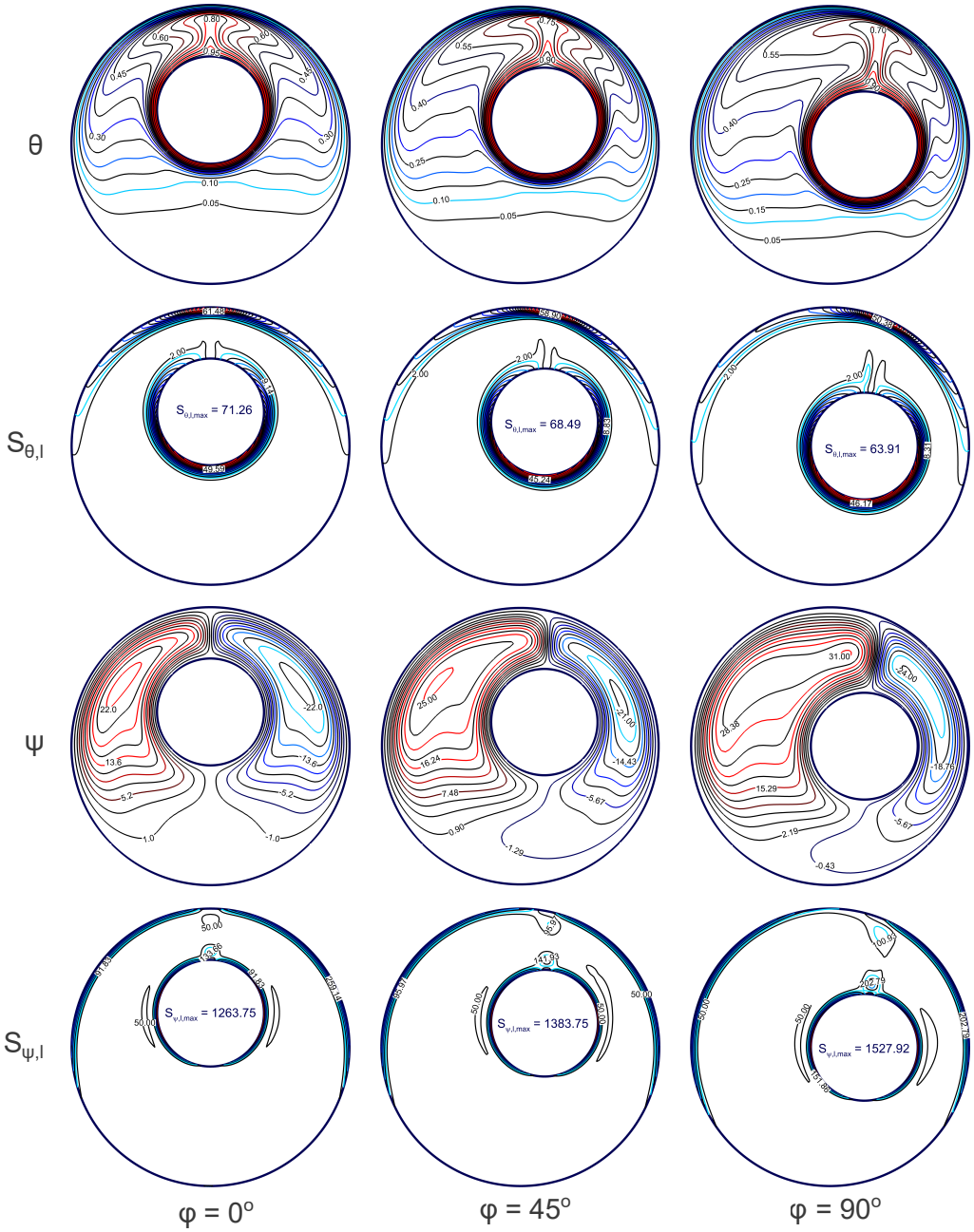

Figure 6. Contours of isotherms (θ), local entropy generation caused by thermal mixing ($S_{\theta,l}$), streamfunction (ψ), and local entropy generation caused by fluid friction ($S_{\psi,l}$) of an eccentric annulus for $\epsilon = 0.4$, $Ra = 10^5$ with different angular positions $\varphi = 0°, 45°, 90°$.

Figure 5 displays the contours of the isotherms, the streamlines, and the entropy generation quantities of an eccentric annulus for $Pr = 10$, $\epsilon = 0.4$, $Ra = 10^3$ with angular positions $\varphi = 0°$, $45°$, $90°$. Because of the influence of the eccentric annulus's angular position, the isotherms and associated plume formation have a slightly curved characteristic at low Ra. All angular points of the isotherms exhibit compression at the top of the outer cold cylinder and the bottom part of the heated inner cylinder. As a result, the top part of the outer cylinder and the bottom portion of the inner cylinder both have the same amount of maximal entropy formation as a result of heat transmission for $\varphi = 0°$ ($S_{\theta,l,max} = 5.46$), $\varphi = 45°$ ($S_{\theta,l,max} = 5.57$), and $\varphi = 90°$ ($S_{\theta,l,max} = 5.57$). The low-magnitude streamfunction illustrates the feeble fluid flow inside the eccentric annulus. At low Ra ($Ra = 10^3$), with an increasing angular position, the fluid flow's intensity rises as $|\psi|_{max} = 2.2,\ 3.63,\ 4.7$ for $\varphi = 0°,\ 45°,\ 90°$, respectively. Because of the significant velocity gradient in the vicinity of

the inner and outer cylinders, where the circulation cells come into contact with the eccentric annulus's cylinders, there is also relatively little entropy formation from fluid friction. For $\varphi = 0°,\ 45°$, and 90°, respectively, the highest value of $S_{\psi,l}$ ($S_{\psi,l,max}$) is determined to be 0.79, 1.29, and 1.73. The local distribution of $S_{\psi,l}$ in these places is indicated by the dense contours of $S_{\psi,l}$ associated with the inner and outer cylinders. Because of the lower velocity gradient, an insignificant $S_{\psi,l}$ is discovered at the eccentric annulus's core for all angular positions ($\varphi = 0°,\ 45°$, and 90°). The left portion of the eccentric annulus experiences the gradual distortion of the isotherms and plume production as Ra rises to 10^4 at $Pr = 10$ and $\epsilon = 0.4$. The commencement of convection also causes an increase in the fluid flow intensity. As seen in Figure 6, the 10^4 convection gradually begins, and the 10^5 convection patterns are intensified.

Convection takes over inside the eccentric annulus when the Ra rises to 10^5, caused by an increase in buoyancy-driven forces. Due to the heightened convection at high Ra (10^5), independent of φ, the isotherms and concomitant plume formation are significantly deformed in the right portion of the eccentric annulus, as shown in Figure 6. Additionally, it is noted that, by comparison with the previous case at $Ra = 10^5$, the generated plumes are compressed at the upper portions of the hot inner cylinder ($0.8 \leq \theta \leq 0.95$ for $\varphi = 0°$, $0.75 \leq \theta \leq 0.95$ for $\varphi = 45°$, $0.7 \leq \theta \leq 0.95$ for $\varphi = 90°$) and the upper portion of the cold outer cylinder ($0.05 \leq \theta \leq 0.50$ for $\varphi = 0°$, $0.05 \leq \theta \leq 0.75$ for $\varphi = 45°$, $0.05 \leq \theta \leq 0.7$ for $\varphi = 90°$). The extremely compressed parts of the temperature distribution at all angular points are the active zones of local entropy formation caused by heat transport. It is observed that near the lower portion of inner cylinder, due to the high temperature gradients in these regions, the highest value of heat-related entropy generation ($S_{\theta,l}, max$) is 71.26 for $\varphi = 0°$, 68.49 for $\varphi = 45°$, and 63.91 for $\varphi = 90°$ (Figure 6). The remaining parts of the eccentric annulus show negligible $S_{\theta,l}$ values because there are fewer temperature gradients, regardless of φ. The streamline structure is discovered to be asymmetrical in terms of the angular positions, akin to the preceding case ($Ra = 10^3$). However, the significance of the streamfunction is greater than in the preceding situation ($Ra = 10^3$) because of the increase in the fluid flow intensity inside the eccentric annulus, as shown by $S_{\psi,l,max} = 22$ for $\varphi = 0°$, $S_{\psi,l,max} = 25$ for $\varphi = 45°$, and $\mid S_{\psi,l,max} = 31$ for $\varphi = 90°$ (see Figure 6). It should be noted that, in comparison to $Ra = 10^3$, there is a larger amount of local entropy production due to fluid friction as $S_{\psi,l,max} = 1263.75, 1383.75$, and 1527.92 occur for $\varphi = 0°, 45°$, and 90°, respectively, at $Ra = 10^5$. In contrast, $S_{\psi,l,max} = 0.79, 1.29$, and 1.73 are found for $\varphi = 0°, 45°$, and 90°, respectively, at $Ra = 10^3$, as illustrated in Figures 5 and 6. Due to the friction between the eccentric annulus and circulation cells, the dense outlines of $S_{\psi,l}$ appear in all upper regions of the annulus, showing the local distribution of $S_{\psi,l}$.

4.3. Case 3: Eccentric Annulus with $\epsilon = 0.8$ and $\varphi = 0°, 45°, 90°$

Figure 7 depicts the contours of the isotherms, the streamlines, and the entropy generation quantities of an eccentric annulus for $Pr = 10$, $\epsilon = 0.8$, $Ra = 10^3$ with angular positions $\varphi = 0°, 45°, 90°$. When the eccentricity is increased from $\epsilon = 0.4$ to $\epsilon = 0.8$, the thermal boundary layer becomes thick and the plume region does not appear inside the annulus. Furthermore, zones with strong temperature gradients are associated with high eccentricity values. The temperature gradient, for example, is substantially larger at $\epsilon = 0.8$ than it is at $\epsilon = 0.4$ (see Figures 5 and 7). The isotherms in the same angular position and in eccentric cylinders are denser than those in concentric cylinders (see Figures 4 and 7). Furthermore, at a low Ra, the isotherms are smooth and monotonic, which illustrates that the heat transfer is primarily due to conduction. Consequently, the maximum local entropy generation due to heat transfer ($S_{\theta,l}, max$) is observed near the inner hot cylinder with the same extent for $\varphi = 0°$ ($S_{\theta,l,max} = 31.66$), $\varphi = 45°$ ($S_{\theta,l,max} = 32.10$) and $\varphi = 90°$ ($S_{\theta,l,max} = 32.06$). The low-magnitude streamfunction illustrates the feeble fluid flow inside the eccentric annulus. The strength of the thermal mixing as well as the fluid flow increases with the angular position as $|\psi|_{max} = 2.2,\ 4.7$, and 6.24 for $\varphi = 0°,\ 45°$, and 90°,

respectively, at $Ra = 10^3$. Because of the significant velocity gradient in the vicinity of the inner and outer cylinders, where the circulation cells come into contact with the eccentric annulus's cylinders, there is also relatively little entropy generation from fluid friction. The maximum value of $S_{\psi,l}$ ($S_{\psi,l,max}$) is observed to be 29.83, 1.38, and 2.16 for $\varphi = 0°, 45°$, and $90°$, respectively

As Ra increases to 10^5, buoyancy forces dominate over viscous forces, leading to enhanced convection in the cavity, and the intensity of the circulation cells is further increased, as seen by the large magnitudes of the streamfunction. For angular positions $\varphi = 0°,\ 45°,\ 90°$, Figure 8 depicts the isotherms, streamlines, heatlines, entropy production due to heat transport, and entropy generation owing to fluid friction for $\epsilon = 0.8$, $Ra = 10^5$. It can be observed that, at a high Ra, the density of the isotherms near the cylinders increases, and the temperature gradients at the surfaces of the cylinders increase. As a result, the heat-related entropy generation magnitudes likewise rise. It is noteworthy that as the angular position grows, $S_{\theta,l,max}$ decreases. According to Figure 8, the maximum values of $S_{\theta,l,max}$ are determined to be 69.81, 62.32, and 58.32 for $\varphi = 0°,\ 45°$, and $90°$, respectively. The middle part of the eccentric annulus has very low values of $S_{\theta,l}$ because there are fewer temperature gradients at all angular positions. It is also noted that the strength of the net circulation surrounding the inner cylinder increases as the Ra rises. For all angular positions, the streamfunction intensity is determined to be higher than $Ra = 10^3$. It should be noted that at $Ra = 10^5$, $|\psi|_{max} = 16.3,\ 23$, and 30 for $\varphi = 0°,\ 45°$, and $90°$, respectively. Since the strength of the fluid flow within the eccentric annulus rises with ϵ and Ra, the magnitude of $S_{\psi,l}$ also increases. For $\varphi = 0°,\ 45°$, and $90°$, the largest amount of entropy generation resulting from fluid friction inside the annulus is $S_{\psi,l,max}$ = 462,625, 1896.47, and 1470.51, respectively. Additionally visible at the walls of the inner and outer cylinders are the active zones of entropy formation caused by fluid friction.

4.4. Quantitative Analysis of Heat Transfer Parameters

Figure 9 shows the variation in the local Nusselt number along the inner and outer cylinders of a concentric annulus with varying Ra ($Ra = 10^3$–10^5) at $\epsilon = 0$ and $\varphi = 0°$. In the case of the inner cylinder, the local Nusselt number at the inner wall (Nu_{lo}^{in}) increases upon increasing the Ra number, i.e., the local heat transfer rate is enhanced. This increase in heat transfer is entirely predictable because of the increased buoyancy force obtained from the temperature difference. It is found that the maximum (Nu_{lo}^{in}) occurs at $\theta = 180°$, which means that the natural convection thermal mixing is more intense in the bottom half of the inner wall. On the other hand, the local Nusselt number at the outer wall (Nu_{lo}^{ou}) is reduced upon increasing the Ra, while the maximum value of (Nu_{lo}^{ou}) is observed at the bottom half of the outer wall. Notably, the minimum value of (Nu_{lo}^{ou}) is found at the ends of the walls, i.e., $\theta = 0°$ and $\theta = 360°$. Figures 10 and 11 display the variation in the local Nusselt number along the inner and outer walls of an eccentric annulus with varying Ra ($Ra = 10^3$–10^5) and angular positions $\varphi = 0°, 45°, 90°$ at two eccentricities $\epsilon = 0.4$ and 0.8, respectively.

Figure 12 shows the variations in the average Nusselt numbers ((Nu_{av}^{in}), Nu_{av}^{ou})) at the inner and outer cylinders of an eccentric annulus at $\epsilon = 0.4$ and $\epsilon = 0.8$ for varying angular positions $\varphi = 0°, 45°, 90°$. It can be observed that in both eccentricity scenarios, the Nu_{av}^{in} at the inner wall increases as the angular positions increase, but the Nu_{av}^{ou} at the outer wall decreases as the angular positions increase. This indicates that when the angle orientations increase, the heat transfer at the inner wall increases. In contrast to $\epsilon = 0.4$, the value of Nu_{av}^{in} is found to be lower in $\epsilon = 0.8$. Similar physics also holds for the Nu_{av}^{ou} situation.

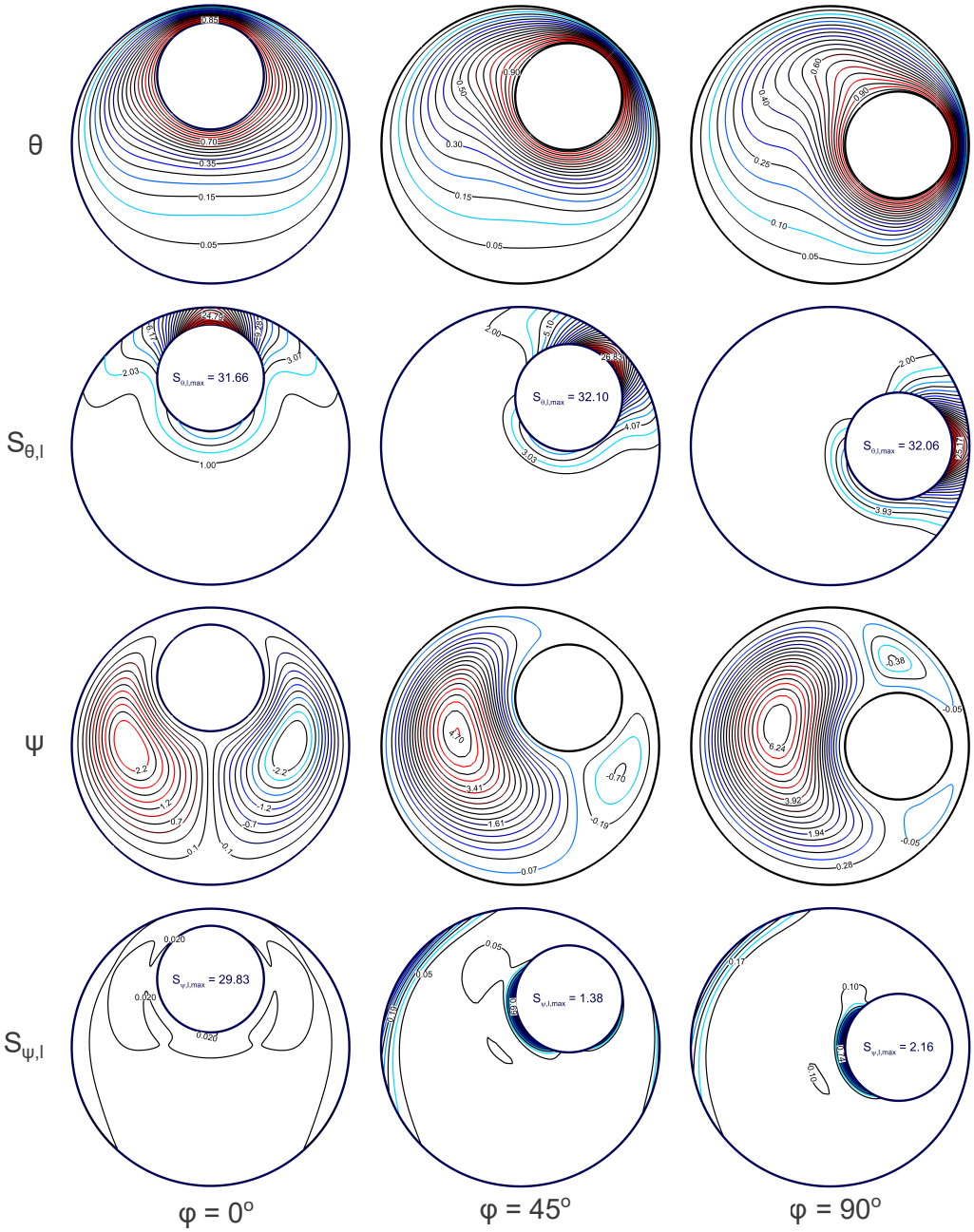

Figure 7. Contours of isotherms (θ), local entropy generation caused by thermal mixing ($S_{\theta,l}$), streamfunction (ψ), and local entropy generation caused by fluid friction ($S_{\psi,l}$) of an eccentric annulus for $\epsilon = 0.8$, $Ra = 10^3$ with different angular positions $\varphi = 0°$, $45°$, $90°$.

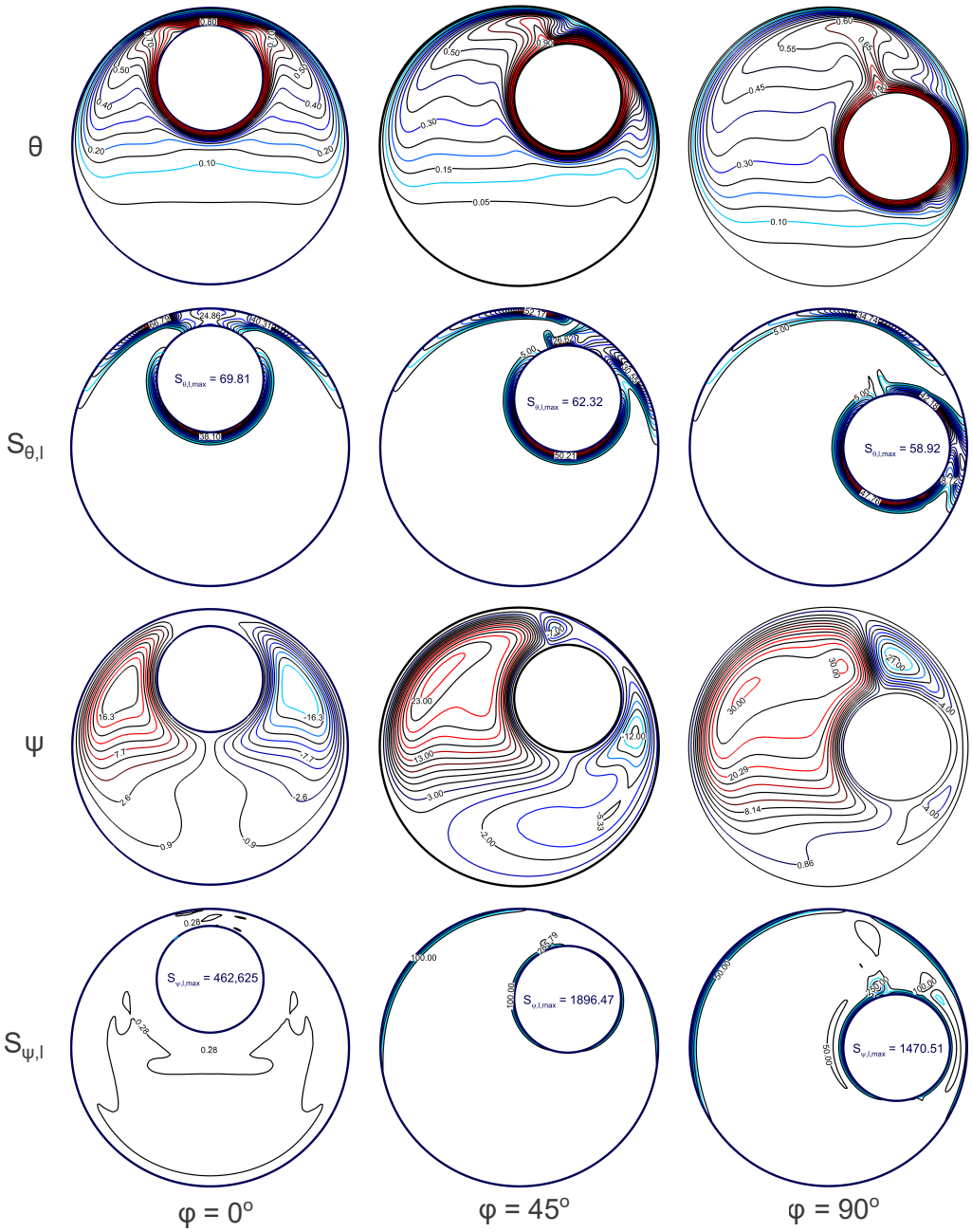

Figure 8. Contours of isotherms (θ), local entropy generation caused by thermal mixing ($S_{\theta,l}$), streamfunction (ψ), and local entropy generation caused by fluid friction ($S_{\psi,l}$) of an eccentric annulus for $\epsilon = 0.8$, $Ra = 10^5$ with different angular positions $\varphi = 0°$, $45°$, $90°$.

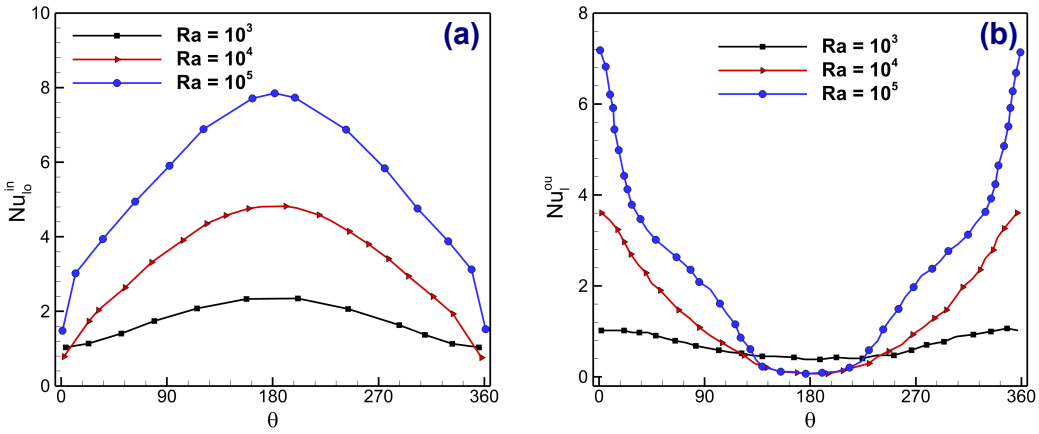

Figure 9. Variation in local Nusselt number at (**a**) inner and (**b**) outer cylinders of a concentric annulus for varying Ra at $\epsilon = 0$, $\varphi = 0°$.

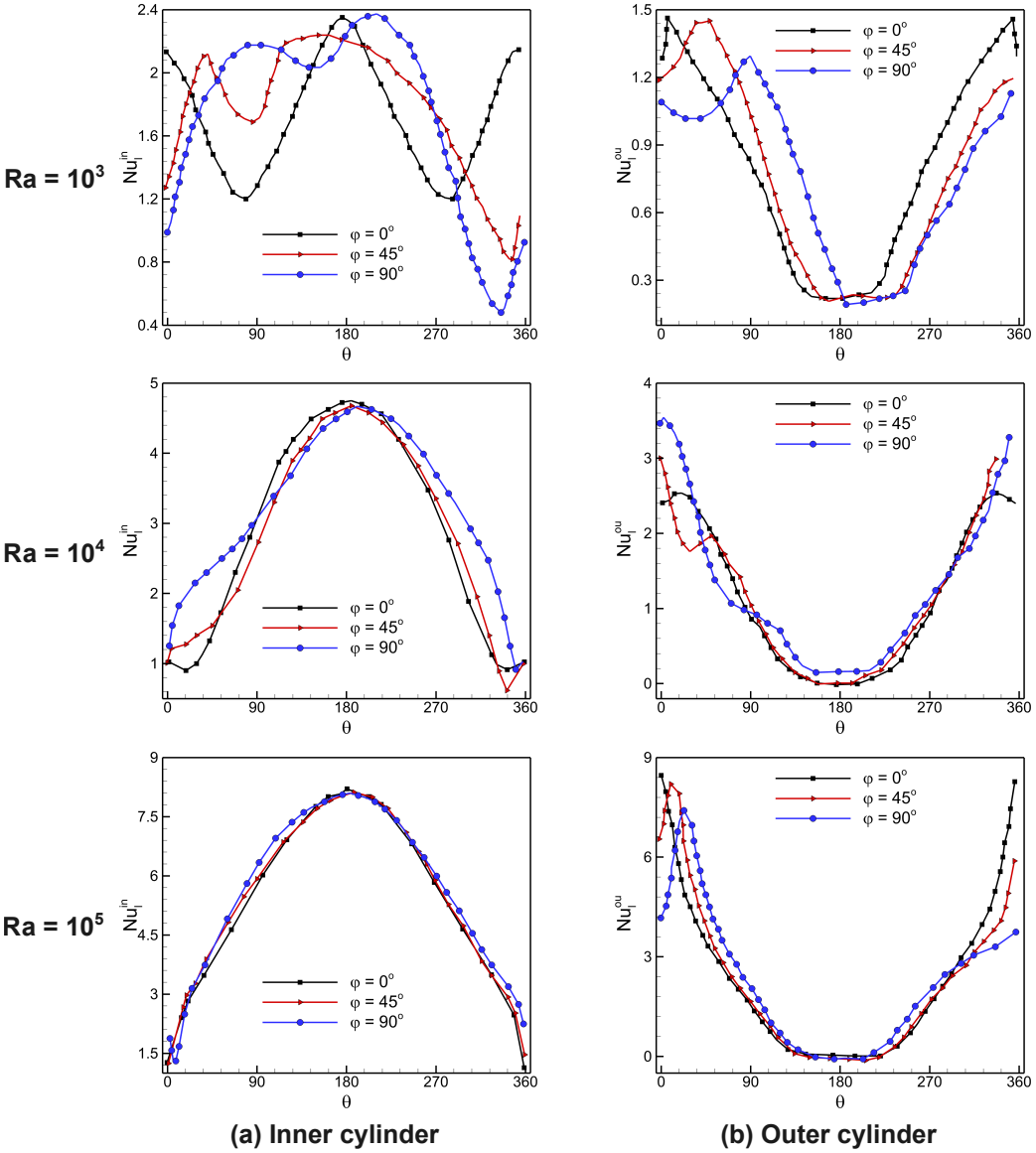

Figure 10. Variation in local Nusselt number at (**a**) inner and (**b**) outer cylinders of an eccentric annulus for varying Ra and angular positions at $\epsilon = 0.4$.

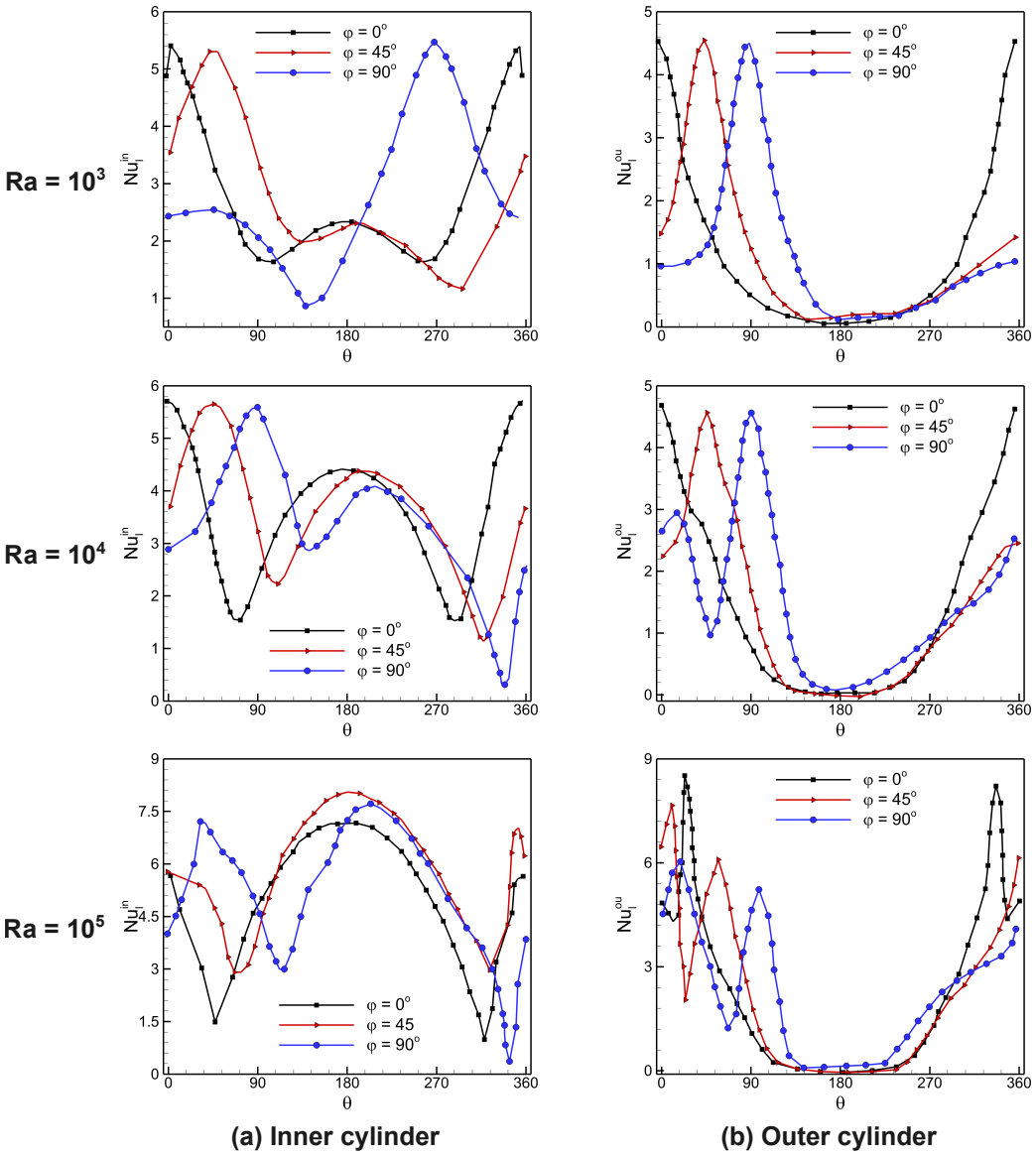

Figure 11. Variation in local Nusselt number at (**a**) inner and (**b**) outer cylinders of an eccentric annulus for varying *Ra* and angular positions at $\epsilon = 0.8$.

Figure 13 illustrates the variation in the circulation intensity ($|\psi|_{max}$) vs. the *Ra* number of an eccentric annulus at $\epsilon = 0.4$ and $\epsilon = 0.8$ for varying angular positions ($\varphi = 0°, 45°, 90°$). The figure shows that the circulation intensity increases as the angular position increases in both eccentricity cases. It can be seen that the $|\psi|_{max}$ value decreases as the ϵ value increases (also see Figures 5–8).

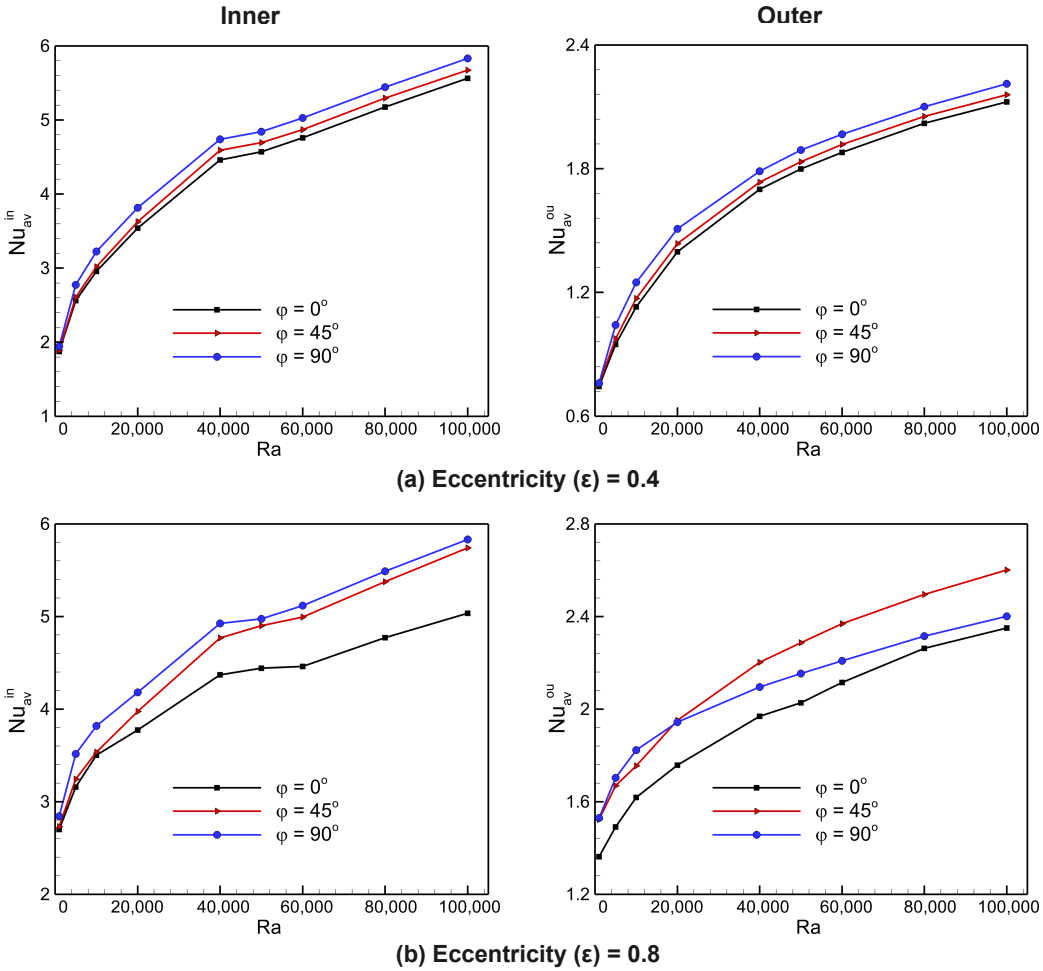

Figure 12. Variations in average Nusselt numbers at inner and outer cylinders of an eccentric annulus at (**a**) $\epsilon = 0.4$, and (**b**) $\epsilon = 0.8$ for varying angular positions $(\varphi = 0°, 45°, 90°)$.

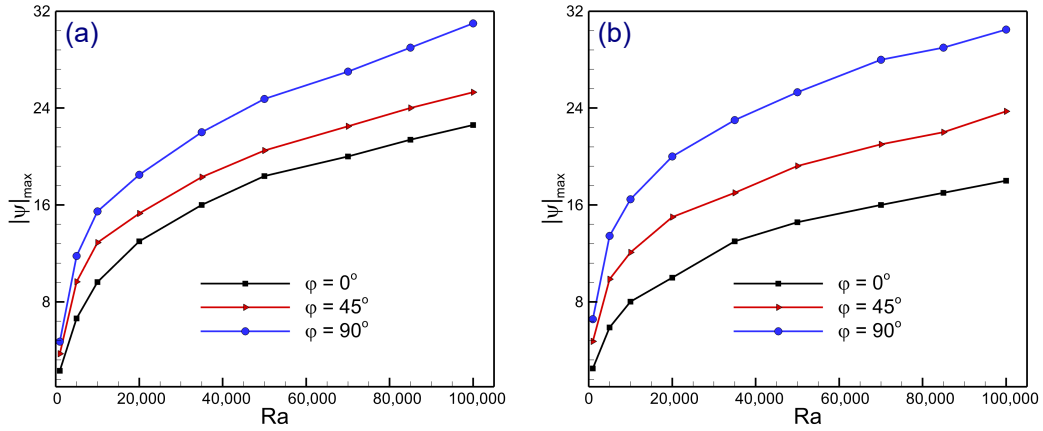

Figure 13. Variation in circulation intensity $(|\psi|_{max})$ vs. Ra number of an eccentric annulus at (**a**) $\epsilon = 0.4$, and (**b**) $\epsilon = 0.8$ for varying angular positions $(\varphi = 0°, 45°, 90°)$.

5. Concluding Remarks and Outlook

The present work provides a computational investigation into the thermal mixing along with the entropy generation throughout the natural convection flow inside an arbitrarily eccentric annulus. The annulus inner wall is heated and maintained at a constant temperature, while the outer wall is cooled and maintained at a constant temperature that is lower than that of the inner wall. The eccentric annulus is filled with salt water. Governing equations are formulated by using the Boussinesq approximation, which are

solved on a structured quadrilateral mesh by using the OpenFOAM software package. The numerical simulations are carried out for Rayleigh number ($Ra = 10^3$–10^5), eccentricity ($\epsilon = 0,\ 0.4,\ 0.8$), angular position ($\varphi = 0^\circ,\ 45^\circ,\ 90^\circ$), and Prandtl number ($Pr = 10$). The quantitative findings are showcased in relation to isotherms (θ), streamlines (ψ), and the formation of local entropy resulting from the irreversibility of heat transfer ($S_{\theta,l}$) and fluid friction ($S_{\psi,l}$). A more thorough examination of the variations in the average Nusselt numbers ($Nu_{av}^{in}, Nu_{av}^{ou}$), local Nusselt numbers ($Nu_{lo}^{in}, Nu_{lo}^{ou}$), and circulation intensity ($|\psi|_{max}$) with varying eccentricities and angular positions within an eccentric annulus is presented. It is found that the eccentricity, angular position, uniform temperature source, and Boussinesq state affect the best state of heat transfer. In addition, the increasing Ra causes an increase in the rate of heat transfer and total entropy generation. It is concluded that an eccentric annulus has a higher rate of heat transfer and entropy generation than a concentric annulus. The results indicate which arrangements and types of eccentric annuli are optimum and may be applicable to all thermal processing operations involving salt fluids.

Our investigation into the impact of eccentricity on thermal mixing may contribute to the development of heat exchangers with higher heat transfer coefficients. This study may be helpful for engineers in controlling the flow patterns and temperature gradients to improve the overall efficiency of the heat exchange between fluids by purposefully creating eccentric annuli within heat exchangers. This optimization can lead to energy savings and improved performance in systems where temperature control is critical. Our findings suggest that eccentric annuli can facilitate more effective cooling by taking advantage of the natural convection processes. For instance, in cooling towers or electronic cooling systems, optimizing the eccentricity and angular positions of components could lead to more uniform temperature distributions and faster heat dissipation from hot surfaces to the cooling medium. This approach may enhance the longevity of equipment and reduce the risk of overheating. Our study also focuses on entropy generation alongside thermal mixing, paying attention to the thermodynamic efficiency of thermal systems. By minimizing entropy generation through optimal design, systems can operate closer to the ideal thermodynamic conditions, reducing energy waste. This aspect is crucial for sustainability goals, as improved efficiency directly translates into reduced energy consumption and lower greenhouse gas emissions for industrial processes. Beyond traditional applications, our study can provide a conceptual basis for the development of thermal devices, which could enhance research on green energy.

The primary objective of this research work was to conduct an analysis of the thermal mixing and entropy generation during natural convection flows within an arbitrary eccentric annulus. The results of this study indicate that the heat and mass transfer in non-Newtonian natural convection flows under different non-uniform thermal boundary conditions is also significantly influenced by thermal mixing and entropy generation. In this context, the present work may be extended to the numerical simulation of thermal mixing and entropy generation in non-Newtonian natural convection flows under different non-uniform thermal boundary conditions in the future.

Author Contributions: Conceptualization, S.S.; software, B.S.; methodology, B.S.; validation, B.S.; formal analysis, S.S.; visualization, S.S. and S.R.; investigation, S.S., B.S. and S.R.; writing—original draft preparation, S.S.; writing—review and editing, S.S., B.S. and S.R.; funding acquisition, S.S. All authors have read and agreed to the published version of the manuscript.

Funding: S.S. acknowledges the partial support provided by the German Research Foundation within the research unit DFG–FOR5409.

Data Availability Statement: Data are contained within the article.

Conflicts of Interest: The authors declare no conflicts of interest.

References

1. Dawood, H.K.; Mohammed, H.A.; Sidik, N.A.C.; Munisamy, K.M.; Wahid, M.A. Forced, natural and mixed-convection heat transfer and fluid flow in annulus: A review. *Int. Commun. Heat Mass Transf.* **2015**, *62*, 45–57. [CrossRef]
2. Rahimi, A.; Saee, A.D.; Kasaeipoor, A.; Malekshah, E.H. A comprehensive review on natural convection flow and heat transfer: The most practical geometries for engineering applications. *Int. J. Numer. Methods Heat Fluid Flow* **2019**, *29*, 834–877. [CrossRef]
3. Geridonmez, B.P.; Oztop, H.F. The effect of inclined periodic magnetic field on natural convection flow of Al_2O_3-Cu/water nanofluid inside right isosceles triangular closed spaces. *Eng. Anal. Bound. Elem.* **2022**, *141*, 222–234. [CrossRef]
4. Barnoon, P. Electroosmotic flow and heat transfer of a hybrid nanofluid in a microchannel: A structural optimization. *Int. J. Thermofluids* **2023**, *20*, 100499. [CrossRef]
5. Geridonmez, B.P.; Oztop, H.F. Conjugate natural convection flow of a nanofluid with oxytactic bacteria under the effect of a periodic magnetic field. *J. Magn. Magn. Mater.* **2022**, *564*, 170135. [CrossRef]
6. Barnoon, P.; Toghraie, D.; Dehkordi, R.B.; Afrand, M. Two phase natural convection and thermal radiation of Non-Newtonian nanofluid in a porous cavity considering inclined cavity and size of inside cylinders. *Int. Commun. Heat Mass Transf.* **2019**, *108*, 104285. [CrossRef]
7. Geridonmez, B.P.; Oztop, H.F. MHD natural convection in a cavity in the presence of cross partial magnetic fields and Al_2O_3-water nanofluid. *Comput. Math. Appl.* **2020**, *80*, 2796–2810. [CrossRef]
8. Beckmann, W. Die Wärmeübertragung in zylindrischen Gasschichten bei natürlicher Konvektion. *Forsch. Geb. Ing. A* **1931**, *2*, 165–178. [CrossRef]
9. Crawford, L.; Lemlich, R. Natural convection in horizontal concentric cylindrical annuli. *Ind. Eng. Chem. Res.* **1962**, *1*, 260–264. [CrossRef]
10. Abbott, M.R. A numerical method for solving the equations of natural convection in a narrow concentric cylindrical annulus with a horizontal axis. *Q. J. Mech. Appl. Math.* **1964**, *17*, 471–481. [CrossRef]
11. Mack, L.R.; Bishop, E.H. Natural convection between horizontal concentric cylinders for low Rayleigh numbers. *Q. J. Mech. Appl. Math.* **1968**, *21*, 223–241. [CrossRef]
12. Moukalled, F.; Acharya, S. Natural convection in the annulus between concentric horizontal circular and square cylinders. *J. Thermophys. Heat Transf.* **1996**, *10*, 524–531. [CrossRef]
13. Powe, R.E.; Carley, C.T.; Carruth, S.L. A Numerical Solution for Natural Convection in Cylindrical Annuli. *J. Heat Transf.* **1971**, *93*, 210–220. [CrossRef]
14. Kuehn, T.H.; Goldstein, R.J. An experimental and theoretical study of natural convection in the annulus between horizontal concentric cylinders. *J. Fluid Mech.* **1976**, *74*, 695–719. [CrossRef]
15. Kumar, R. Study of natural convection in horizontal annuli. *Int. J. Heat Mass Transf.* **1988**, *31*, 1137–1148. [CrossRef]
16. Labonia, G.; Guj, G. Natural convection in a horizontal concentric cylindrical annulus: Oscillatory flow and transition to chaos. *J. Fluid Mech.* **1998**, *375*, 179–202. [CrossRef]
17. Dyko, M.P.; Vafai, K.; Mojtabi, A.K. A numerical and experimental investigation of stability of natural convective flows within a horizontal annulus. *J. Fluid Mech.* **1999**, *381*, 27–61. [CrossRef]
18. Lshahrani, D.; Zeitoun, O. Natural convection in horizontal cylindrical annuli with fins. *Alex. Eng. J.* **2005**, *44*, 825–837.
19. Teertstra, P.; Yovanovich, M.M.; Culham, J.R. Analytical modeling of natural convection in concentric spherical enclosures. *J. Thermophys. Heat Transf.* **2006**, *20*, 297–304. [CrossRef]
20. Sankar, M.; Venkatachalappa, M.; Shivakumara, I.S. Effect of magnetic field on natural convection in a vertical cylindrical annulus. *Int. J. Eng. Sci.* **2006**, *44*, 1556–1570. [CrossRef]
21. Alsabery, A.I.; Naganthran, K.; Azizul, F.M.; Hashim, I.; Nazar, R. Numerical study of conjugate natural convection heat transfer of a blood filled horizontal concentric annulu. *Int. Commun. Heat Mass Transf.* **2020**, *114*, 104568. [CrossRef]
22. Rana, S.; Sengupta, B.; Singh, S. Natural convection study in cylindrical annulus through OpenFOAM. In *Computational Fluid Flow and Heat Transfer Advances, Design, Control, and Applications*; CRC Press: Boca Raton, FL, USA, 2024.
23. Trombetta, M.L. Laminar forced convection in eccentric annuli. *Int. J. Heat Mass Transf.* **1971**, *14*, 1161–117. [CrossRef]
24. Kuehn, T.H.; Goldstein, R.J. An experimental study of natural convection heat transfer in concentric and eccentric horizontal cylindrical annuli. *J. Heat Transf.* **1978**, *100*, 635–640. [CrossRef]
25. Chakrabarti, S.; Probert, S.D.; Shilston, M.J. Optimal eccentric annuli (containing atmospheric-pressure air) for thermally insulating, horizontal, relatively cold pipes. *Appl. Energy* **1983**, *14*, 257–293. [CrossRef]
26. Badr, H.M. Study of laminar free convection between two eccentric horizontal tubes. *Trans. Can. Soc. Mech. Eng.* **1983**, *7*, 190–197. [CrossRef]
27. Prusa, J.; Yao, L.S. Natural convection heat transfer between eccentric horizontal cylinders. *J. Heat Transf.* **1983**, *105*, 108–116. [CrossRef]
28. Guj, G.; Iannetta, S.; Moretti, G. Experimental analysis of thermal fields in horizontally eccentric cylindrical annuli. *Exp. Fluids* **1992**, *12*, 385–393. [CrossRef]
29. Guj, G.; Stella, F. Natural convection in horizontal eccentric annuli: Numerical study. *Numer. Heat Transf. A* **1995**, *27*, 89–105. [CrossRef]
30. Shu, C.; Yao, Y.; Yeo, K.S.; Zhu, Y.D. Numerical analysis of flow and thermal fields in arbitrary eccentric annulus by differential quadrature method. *Heat Mass Transf.* **2002**, *38*, 597–608. [CrossRef]

31. Mahfouz, F.M. Natural convection within an eccentric annulus at different orientations. *J. Thermophys. Heat Trans.* **2012**, *26*, 665–672. [CrossRef]
32. Yuan, X.; Tavakkoli, F.; Vafai, K. Analysis of natural convection in horizontal concentric annuli of varying inner shape. *Numer. Heat Transf. Part A Appl.* **2015**, *68*, 1155–1174. [CrossRef]
33. Talukdar, D.; Tsubokura, M. Numerical study of natural-convection from horizontal cylinder at eccentric positions with change in aspect ratio of a cooled square enclosure. *Heat Mass Transf.* **2022**, *58*, 849–871. [CrossRef]
34. Shahsavar, A.; Noori, S.; Toghraie, D.; Barnoon, P. Free convection of non-Newtonian nanofluid flow inside an eccentric annulus from the point of view of first-law and second-law of thermodynamics. *ZAMM* **2021**, *101*, e202000266. [CrossRef]
35. Al-Sumaily, G.F.; Hussen, H.M.; Chaichan, M.T.; Dhahad, H.A.; Thompson, M.C. Numerical analysis of the effect of porous structure on free convection heat transfer inside an eccentric annular space. *Therm. Sci. Eng. Prog.* **2023**, *37*, 101579. [CrossRef]
36. Bejan, A. *Entropy Generation Minimization*; CRC Press: Boca Raton, FL, USA, 1982.
37. Mahmud, S.; Fraser, R.A. Analysis of entropy generation inside concentric cylindrical annuli with relative rotation. *Int. J. Therm. Sci.* **2003**, *42*, 513–521. [CrossRef]
38. Haddad, O.M.; Alkam, M.K.; Khasawneh, M.T. Entropy generation due to laminar forced convection in the entrance region of a concentric annulus. *Energy* **2004**, *29*, 35–55. [CrossRef]
39. Yari, M. Second-law analysis of flow and heat transfer inside a microannulus. *Int. Commun. Heat Mass Transf.* **2009**, *36*, 78–87. [CrossRef]
40. Chen, S.; Liu, Z.; Bao, S.; Zheng, C. Natural convection and entropy generation in a vertically concentric annular space. *Int. J. Therm. Sci.* **2010**, *49*, 2439–2452. [CrossRef]
41. OpenFOAM. OpenFOAM Project Web Page of the OpenCFD LTD. 2022. Available online: https://www.openfoam.com (accessed on 31 December 2023)
42. Singh, A.K.; Roy, S.; Basak, T. Analysis of Bejan's heatlines on visualization of heat flow and thermal mixing in tilted square cavities. *Int. J. Heat Mass Transf.* **2012**, *55*, 2965–2983. [CrossRef]